Frequency Doubled High-Power Semiconductor Disk Lasers for Projection and Ion-Trapping Applications

Alexander Hein

We present optically pumped semiconductor disk lasers (OPSDLs) emitting in the 900–1100 nm band which are frequency doubled to access the visible spectrum. In particular, we focus on presenting the design, fabrication, and specific characteristics. Fundamental outputs exceeding 25 W and visible radiation with powers greater than 11 W are achieved. The blue and green emission at wavelengths around 450–470 and 520–540 nm yield advantageous gamuts for projection applications. Moreover, other accessible wavelengths in this spectral region, e.g. 493 nm, single frequency operation, and the good beam quality of these devices enable optical ion trapping experiments.

1. Introduction

Optically pumped semiconductor disk lasers, also called vertical-external-cavity surface-emitting lasers (VECSELs), are a relatively novel class of semiconductor lasers which combine high output powers and excellent beam qualities [1, 2]. The basic principle of a semiconductor disk laser is illustrated in Fig. 1. The semiconductor disk, which is mounted on a heat spreader and a heat sink, forms a stable resonator together with the external concave mirror. Optical pumping of the semiconductor disk is provided by a pump laser system equipped with fiber coupled broad-area edge-emitting laser diodes. More complex cavities with additional external mirrors, miniaturized systems, as well as multiple-chip resonators have been realized [3]. The easily accessible external resonator and high intra-cavity field intensities make OPSDLs highly suitable for the generation of higher harmonics. Combining epitaxial structures from the well established AlGaAs-GaAs-InGaAs material system and second-harmonic (SH) generation, wavelengths in the visible spectrum starting from blue [4,5], green [4,6] to yellow [7] with high optical outputs can be addressed. Frequency-quadrupled systems reaching into the UV for environmental sensing, chemical detection, and lidar application, as well as for high-resolution spectroscopy [8, 9] and ion cooling [10] were also demonstrated and attract more and more interest.

Moreover, semiconductor disk lasers have not only unsurpassed freedom in the choice of the emission wavelength. Since design and material composition of the epitaxial structure can be widely varied and drawing on the fact that absorption in the semiconductor material above the band gap is extremely high and not limited to a very narrow band, optical pumping is not limited to discrete wavelengths [11], and the spectral requirements for the pump sources are drastically reduced as compared to diode-pumped solid-state lasers.

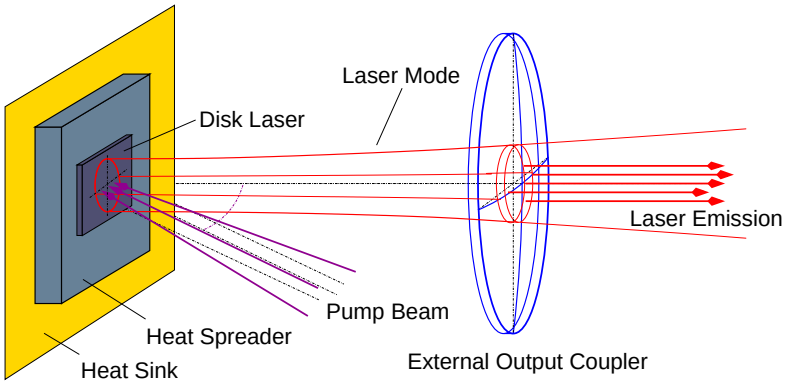

Fig. 1: Schematic illustration of a semiconductor disk laser. The stable hemispheric laser resonator consisting of the semiconductor disk and an external concave mirror provides fundamental transverse-mode operation.

Being able to tailor the wavelength, these devices are suited as illumination sources in stereoscopic 3D-projection [12] since the required channel separation can be achieved without sacrificing the optimum gamuts. Here, especially the green spectral region (520–540 nm) is of interest, but also the blue and red bands can be realized with OPSDL technology [3]. Furthermore, the cyan emission around 493 nm enables optical trapping of Ba-ions since this laser line is on resonance with the atomic transition. The presented work is focused on the design, fabrication and respective characteristics of 520 and 493 nm emitting VECSELs.

2. Design and Fabrication

2.1 Layer design

Key elements in the layer design are a dielectric anti-reflection (AR) coating, a resonant periodic gain (RPG) structure, and a rear distributed Bragg reflector (DBR). The layer structure is depicted in more detail in Fig. 2. For the DBR an alternating stack of 56 $Al_{0.15}Ga_{0.85}As$/AlAs layers was chosen. With this material configuration, the DBR provides a high reflectivity for the emission wavelength ($R > 99.9\,\%$) but is non-absorbing for the pump wavelength of 804 nm. The absorption of the pump radiation only takes place in the gain region while all other layers are optically transparent.

Due to the transparency of the DBR and a Ti/Au metalization which terminates the semiconductor layer structure, the pump light is reflected back into the active region, thus, providing a resonant pumping condition. There is decay originating from absorption in the GaAs capping layer and the Ti layer, hence, these layers should be kept rather thin. An alternative approach to the metal reflector is to utilize a double-band DBR, providing high reflectivities for both the emission and the pump wavelength [5, 13]. Targeting wavelengths beyond 1 µm, such structures with two highly reflecting bands will result in an increased thermal impedance and demand a more complex epitaxial growth [14]. As illustrated on the right hand side of Fig. 2, the semiconductor surface is located in a

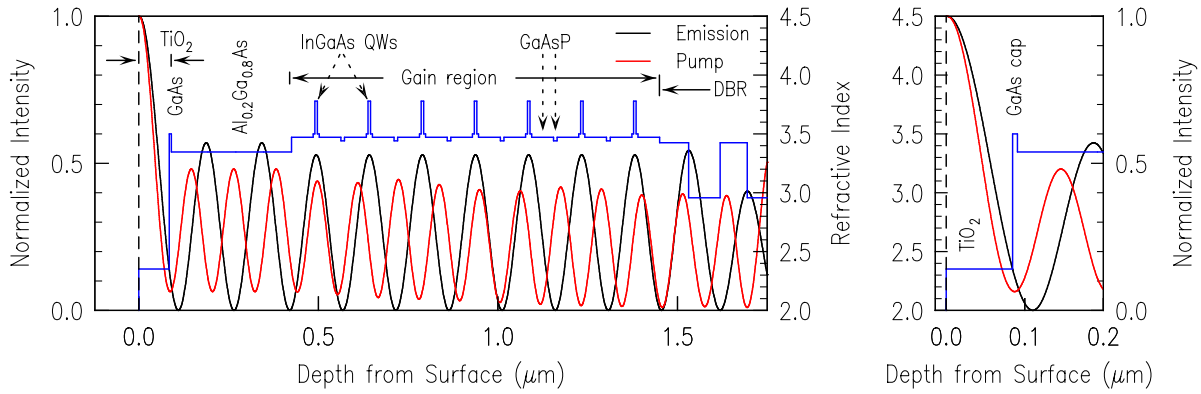

Fig. 2: Layer structure of a device designed for an emission wavelength of 1040 nm. The Bragg reflector is indicated with the first couple of mirror pairs. The interface semiconductor/dielectric is shown in more detail. The node position of the field intensity for the two respective wavelengths is located at the semiconductor/dielectric interface where absorption is reduced to a minimum.

node of the electric-field intensity of the standing-wave patterns. Due to surface states inside the band gap, the semiconductor surface would exhibit high optical absorption for the pump light and also for the laser light ($\lambda < 1\,\mu$m) at this position. Our approach to circumvent the high absorption is a quarter-wavelength dielectric surface coating on the semiconductor surface [15]. For one, the layer serves as an AR-coating for the pump wavelength and passivates the surface, on the other hand the interface absorption is minimized by relocating the antinode. Spectral characteristics of a device designed for 1040 nm emission are summarized in Fig. 3. Due to the separation of the excitonic dip and the subcavity resonance in the reflectivity spectra [6] by varying the angle of incidence, the spectral behavior can be fully analyzed. The photoluminescence (PL) measurements provide the optimum operating temperature when the PL of the QWs has the best overlap with the subcavity resonance.

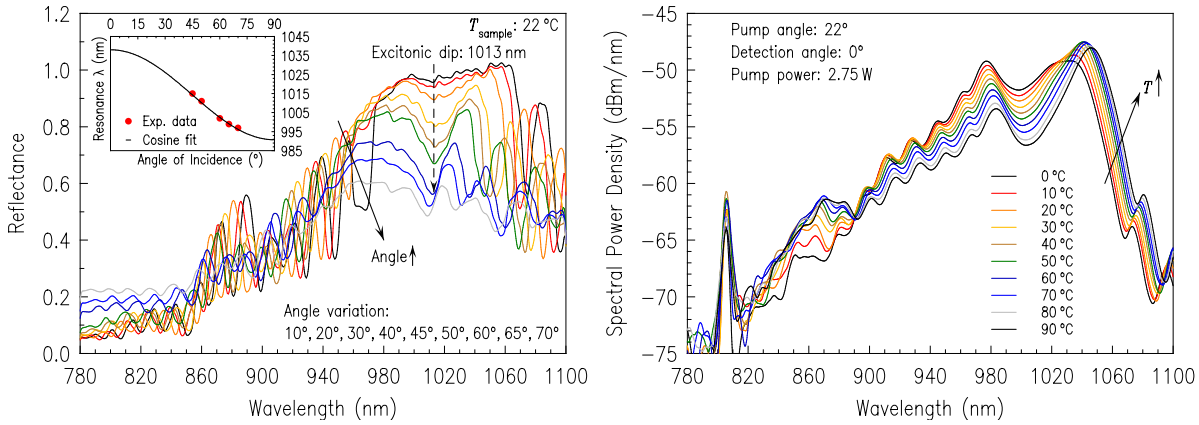

Fig. 3: Angle resolved reflectivity spectra (left) and temperature dependent surface photoluminescence (right).

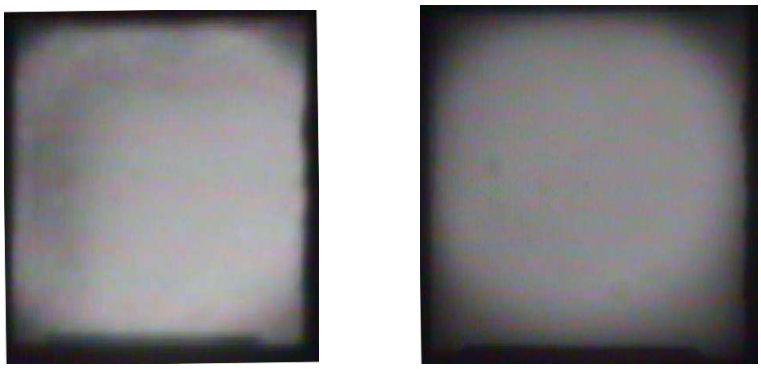

Fig. 4: Locally resolved photoluminescence of a 1.5 mm×1.8 mm disk laser before (left) and after (right) operation, where possible crystal defects could be visualized as dark lines or a dark cross-hatch pattern.

A further and probably most important point that has to be addressed is the strain in the semiconductor structure. Incorporating indium into the QWs results in pseudomorphic growth of the crystal lattice which is more and more compressively strained. Although strained QWs show clear advantages in gain characteristics [16], relaxations of these layers result in line defects of the crystal structure. Compensation of the compressive strain from the InGaAs QWs was realized by tensilely strained GaAsP barriers. In order not to create a strong strain gradient at the well/barrier interface a step of pure GaAs was introduced as a mediator. The structural quality of the devices can be easily assessed by local photoluminescence where the full chip area is excited with the pump laser. Figure 4 shows a locally resolved photoluminescence picture of a device before and after operation at an output power in excess of 20 W that has no defect dislocations at all. Efficient and long-living semiconductor disk lasers should be completely free of these line defects.

2.2 Mounting and processing

The devices were grown in reverse order – RPG first, DBR last – by solid-source molecular beam epitaxy (MBE) on (100)-oriented GaAs substrates and soldered upside-down onto heat spreaders and heat sinks with indium. The soldering happens in an inert nitrogen atmosphere where formic acid is added temporarily as a suitable flux for indium. Afterwards, the substrate is removed by wet-chemical etching leaving only the epitaxially grown layer stack [17]. Precise etching control is achieved with a sequence of etch stop layers (AlAs/GaAs/AlAs) with high selectivities for the respective etchants. On the left hand side of Fig. 5 a scanning electron microscope (SEM) image of an upside-down mounted device with substrate is shown. In operation, the generated heat is spread by the chemically vapor deposited (CVD) diamond and transfered to the heat sink. Alternatively, optically transparent diamond with high thermal conductivity can be used to remove the heat from the front side of the as-grown disk lasers [7]. The right part of Fig. 5 shows a processed chip with the substrate and etch stop layers fully removed exposing the capping layer. The dielectric coating is applied in the final step.

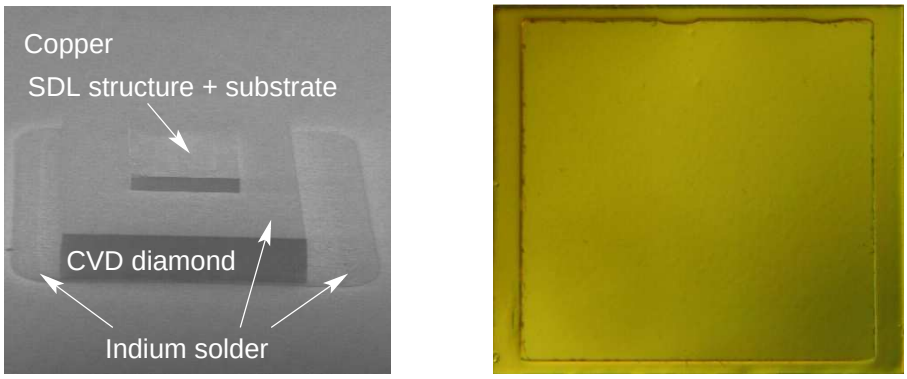

Fig. 5: SEM image of an upside-down soldered SDL structure with substrate on a diamond heat spreader and copper heat sink (left) and the surface photograph of a fully processed laser chip after substrate removal (right).

3. Characterization

3.1 Fundamental regime

The devices were tested in a straight cavity with a curved output coupler having a radius of curvature of -150 mm. The SDL structure was pumped by a fiber coupled module with an emission around 804 nm into a spot of approximately 500 μm diameter confirmed by measuring the illuminated area. The pump light was incident at an angle of 22° to the chip surface normal giving a slight ellipticity. The temperature was controlled with a commercial thermoelectric Peltier cooler. The Peltier element in turn was contact cooled via a copper mount with running water. At a heat sink temperature of 17 °C, more than 25 W of output power were generated in transverse multi-mode operation with a slope efficiency close to 50 % as depicted in Fig. 6. The devices are capable of operating at heat sink temperatures of 90 °C with optical outputs of up to 3.5 W and slope efficiencies of 25 % [19]. Throughout the whole operation range, we observed an almost constant absorptance of 91 % of the pump power. This high degree of absorptance underlines the importance of the dielectric surface coating and the metal reflector completing the DBR in order to increase the overall efficiency. The overall efficiency (incident power-to-output power) for optical outputs around 20 W was 40–43 %. The increase of the wavelength with absorbed pump power was 0.13 nm/W indicating good heat conduction, and the total wavelength shift was approximately 7 nm from threshold to power saturation as indicated by the spectra in the inset.

3.2 Second-harmonic regime

The external cavity of OPSDLs allows efficient intra-cavity SH generation due to high field intensities inside the resonator. Figure 7 shows the cavity setup of a folded resonator with nonlinear crystal and birefringent quartz filter plate (BRF) [6] tilted to the Brewster angle for linear polarization. This resonator configuration with the folding mirror located

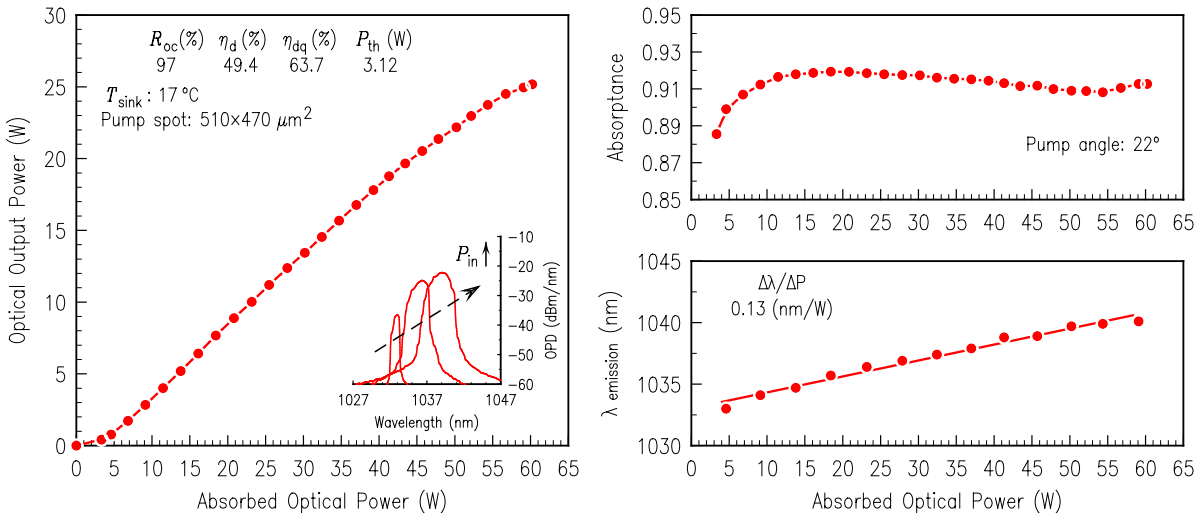

Fig. 6: Output power characteristics of a semiconductor disk laser designed for an emission at 1040 nm. The pumped spot size was $510 \times 470\,\mu\text{m}^2$. The device was operated with an output coupler reflectivity of 97 %.

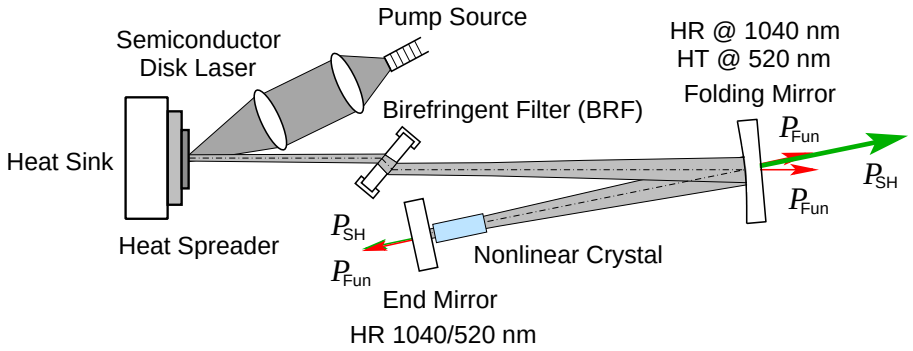

Fig. 7: Schematic setup of a folded V-type cavity for second-harmonic generation. Wavelength and polarization control are realized by the use of a birefringent quartz filter plate tilted to the Brewster angle.

further away from the disk laser than twice the focal length of the mirror yields a strong reduction of the beam waist in the nonlinear crystal in order to achieve higher intensities.

3.3 Green-emitting OPSDLs for stereo projection

Using the cavity setup illustrated in Fig. 7, we have obtained an output power in excess of 11 W and conversion efficiencies of 23 % at a wavelength of 519 nm. The output characteristic is provided in Fig. 8. The frequency conversion was realized by type-I critical phase-matching. The nonlinear 11 mm-long lithium triborate (LBO) crystal was stabilized to a temperature of 40 °C while the heat-sink temperature was 17 °C. Control and narrowing of the emission wavelength was realized by rotating a 2 mm-thick BRF plate.

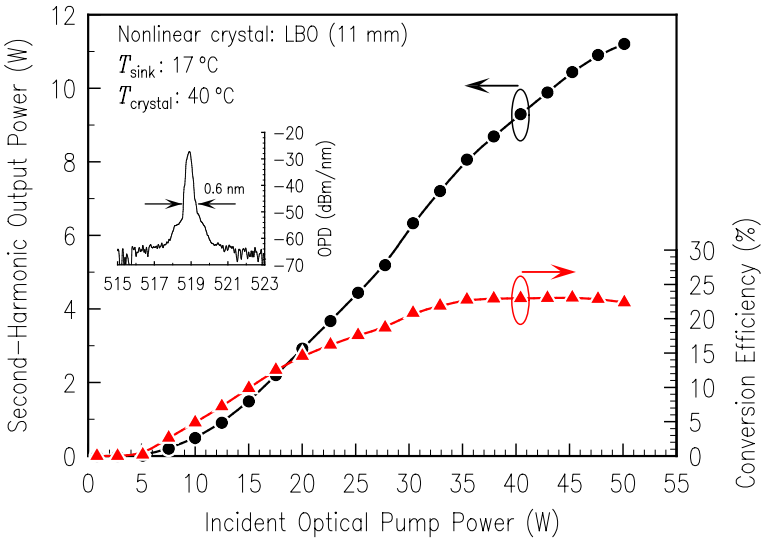

Fig. 8: Output power characteristic and emission spectrum of the second-harmonic emission of a frequency-doubled semiconductor disk laser at 519 nm. A maximum output power of 11.2 W and a conversion efficiency of 23 % with respect to the incident pump power were achieved.

3.4 Cyan-emitting OPSDLs for ion trapping

For off-resonance trapping of the Ba-ion an emission wavelength of 493.3 nm is desirable, which is a couple of 100 GHz detuned with respect to the $6S_{1/2}$-$6P_{1/2}$ transition, as indicated in Fig. 9. This optical trap prevents the longitudinal micro-motion of the 138Ba-ion while the transverse micro-motion is foreclosed by a Paul trap. To address this, OPSDLs with a fundamental emission around 986.6 nm are required and should deliver watt-level power in the second-harmonic regime at a good beam quality. Further, the linewidth should be restricted to smaller values than 1 GHz and the source must operate on a single longitudinal mode. OPSDL devices intrinsically show narrow linewidth behavior of the individual peaks capable of delivering widths in the kHz-range. However, due to relatively long resonators and the consequent small mode spacing, typically pm-range, true single-frequency operation demands additional elements for frequency stabilization, or an active stabilization of the cavity is required [9]. We modified an OPSDL structure that was originally designed for an emission at 976 nm with a thicker dielectric coating to red-shift the emission. Fig. 10 shows the second-harmonic output characteristics of this device. It should be noted that here the device was directly mounted on a gold-platted copper heat sink, and no CVD diamond heat spreader was used. Detuning the laser from its optimum wavelength of 979.5 nm to the trap wavelength of 986.6 nm with a 4 mm thick BRF resulted in a power penalty for the SH of about 1.3 W. After insertion of an uncoated yttrium aluminum garnet (YAG) etalon to obtain single-frequency operation, the SH output power further dropped to roughly 500 mW. The corresponding spectra are depicted in the top-right part of Fig. 10. The poor conversion efficiency of about 2.5 % is a result of detuning the fundamental laser line by more than 7 nm from optimal conditions and insufficient thermal management.

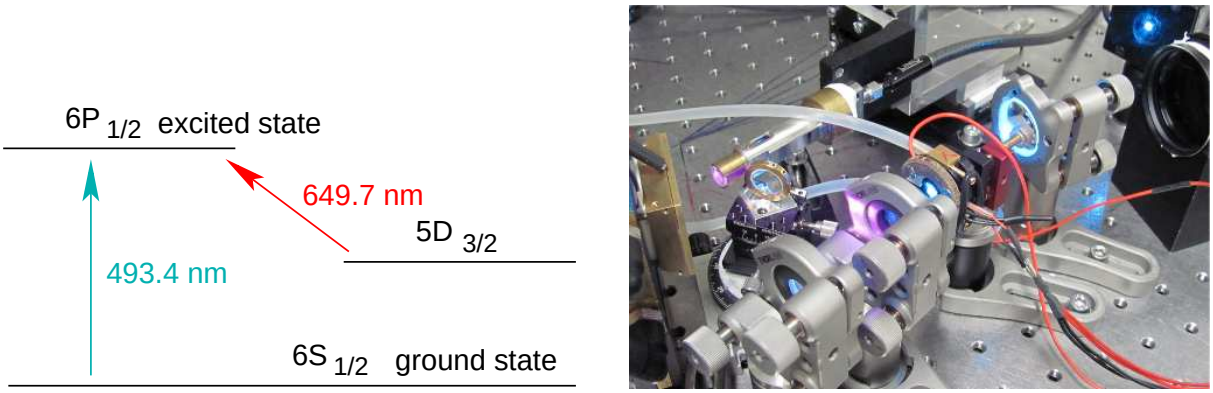

Fig. 9: Laser transitions for the 138Ba ion (left). V-type cavity arrangement for a frequency doubled OPSDL with two concave external mirrors incorporating a BRF, a solid YAG etalon, and a nonlinear crystal with temperature stabilization to generate single-frequency emission at 493.3 nm (right).

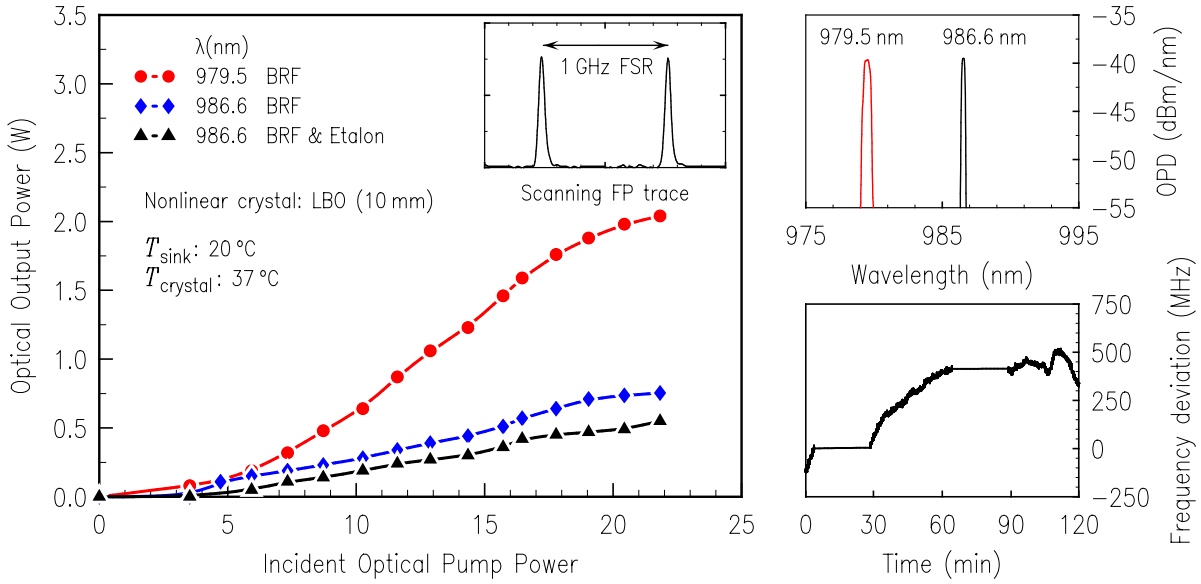

Fig. 10: Left: Frequency doubled output of the ion trap OPSDL. The inset shows the frequency spectrum obtained with a scanning Fabry–Pérot interferometer confirming single-frequency operation and linewidth of approximately 40 MHz. Right: Optical spectra (top) and frequency behavior over time (bottom).

Single-frequency operation was analyzed with a scanning Fabry–Pérot interferometer having a FSR of 1 GHz as indicated in the inset. Even though the setup was not shielded from external disturbances we observed single-frequency operation throughout the whole operation range with a linewidth of approximately 40 MHz. The linewidth could be reduced to 25 MHz by decresing the water throughput for cooling. Further, the frequency deviation from the reference value of 303.6448 THz on a time scale of two hours was only slightly more than 500 MHz, and thus, well within the experiment-required specifications.

4. Conclusion

We demonstrated frequency doubled optically pumped semiconductor disk lasers that are highly suitable for projection applications and off-resonance trapping of ions. Our results and works published by other groups with further frequency conversion show that this type of lasers with its unmatched flexibility in addressing wavelengths from the UV to the mid IR and its tuning abilities can become a well-established technology in a large variety of laser-based optical systems.

Acknowledgment

The assistance of Susanne Menzel and Rudolf Rösch with growth and device processing as well as of Andreas Ziegler with various measurements is gratefully acknowledged.

References

[1] M. Kuznetsov, F. Hakimi, R. Sprague, and A. Mooradian, "Design and characteristics of high-power (>0.5-W CW) diode-pumped vertical-external-cavity surface-emitting semiconductor lasers with circular TEM_{00} beams," *IEEE J. Select. Topics Quantum Electron.* vol. 5, no. 3, pp. 561–573, 1999.

[2] O.G. Okhotnikov (Ed.), *Semiconductor Disk Lasers – Physics and Technology*, Wiley-VCH, Weinheim, 2010.

[3] S. Calvez, J.E. Hastie, M. Guina, O.G. Okhotnikov, and M.D. Dawson, "Semiconductor disk lasers for the generation of visible and ultraviolet radiation," *Laser and Photon. Rev.* vol. 3 no. 5, pp. 407–434, 2009.

[4] L.E. Hunziker, C. Ihli, and D.S. Steingrube, "Miniaturization and power scaling of fundamental mode optically pumped semiconductor lasers," *IEEE J. Select. Topics Quantum Electron.* vol. 13, no. 3, pp. 610–618, 2007.

[5] A. Hein, F. Demaria, A. Kern, S. Menzel, F. Rinaldi, R. Rösch, and P. Unger, "Efficient 460-nm second-harmonic generation with optically pumped semiconductor disk lasers," *IEEE Photon. Technol. Lett.* vol. 23, no. 3, pp. 179–181, 2011.

[6] A. Hein, S. Menzel, and P. Unger, "High-power high-efficiency optically pumped semiconductor disk lasers in the green spectral region with a broad tuning range," *Appl. Phys. Lett.* vol. 101, pp. 111109-1–4, 2012.

[7] W.J. Alford, G.J. Fetzer, R.J. Epstein, Sandalphon, N. Van Lieu, S. Ranta, M. Tavast, T. Leinonen, and M. Guina, "Optically pumped semiconductor lasers for precision spectroscopic applications," *IEEE J. Quantum Electron.* vol. 49, no. 8, pp. 719–727, 2013.

[8] Y. Kaneda, M. Fallahi, J. Hader, J.V. Moloney, S.W. Koch, B. Kunert, and W. Stolz, "Continuous-wave single-frequency 295 nm laser source by a frequency-quadrupled optically pumped semiconductor laser," *Opt. Lett.* vol. 34, no. 22, pp. 3511–3513, 2009.

[9] J. Paul, Y. Kaneda, T.L. Wang, C. Lytle, J.V. Moloney, and R.J. Jones, "Doppler-free spectroscopy of mercury at 253.7 nm using a high-power, frequency-quadrupled, optically pumped external-cavity semiconductor laser," *Opt. Lett.* vol. 36, no. 1, pp. 61–63, 2011.

[10] S. Ranta, M. Tavast, T. Leinonen, R. Epstein, and M. Guina, "Narrow linewidth 1118/559 nm VECSEL based on strain compensated GaInAs/GaAs quantum wells for laser cooling of Mg-ions," *Opt. Mater. Exp.* vol. 2, no. 8, pp. 1011–1019, 2012.

[11] S. Haupt, M. Furitsch, H.H. Lindberg, I. Pietzonka, U. Strauß, and G. Bacher, "Analysis of the pump wavelength dependence of a 1060-nm VECSEL," *IEEE Photon. Technol. Lett.* vol 24, no. 5, pp. 341–343, 2012.

[12] H. Jorke, A. Simon, and M. Fritz, "Advanced stereo projection using interference filters," *J. Soc. Inf. Disp.* vol. 17, no. 5, pp. 407–410, 2009.

[13] K.-S. Kim, J. Yoo, Kim, G., S. Lee, S. Cho, J. Kim, T. Kim, and Y. Park, "Enhancement of pumping efficiency in a vertical-external-cavity surface-emitting laser," *IEEE Photon. Technol. Lett.* vol. 19, no. 23, pp. 1925–1927, 2007.

[14] L. Fan, C. Hessenius, M. Fallahi, J. Hader, H. Li, J.V. Moloney, W. Stolz, S.W. Koch, J.T. Murray, and R. Bedford, "Highly strained InGaAs/GaAs multiwatt vertical-external-cavity surface-emitting laser emitting around 1170 nm," *Appl. Phys. Lett.* vol. 91, pp. 131114-1–3, 2007.

[15] F. Demaria, S. Lorch, S. Menzel, M.C. Riedl, F. Rinaldi, R. Rösch, and P. Unger, "Design of highly efficient high-power optically pumped semiconductor disk lasers," *IEEE J. Select. Topics Quantum Electron.* vol. 15, no. 3, pp. 973–977, 2009.

[16] L.A. Coldren and S. Corzine, *Diode Lasers and Photonic Intergrated Circuits*, John Wiley & Sons Inc., New York, 1995.

[17] E. Gerster, I. Ecker, S. Lorch, C. Hahn, S. Menzel, and P. Unger, "Orange-emitting frequency-doubled GaAsSb/GaAs semiconductor disk laser," *J. Appl. Phys.* vol. 94, no. 12, pp. 7397–7401, 2003.

[18] B. Heinen, T.-L. Wang, M. Sparenberg, A. Weber, B. Kunert, J. Hader, S.W. Koch, J.V. Moloney, M. Koch, and W. Stolz, "106 W continuous-wave output power from vertical-external-cavity surface-emitting laser," *Electron. Lett.* vol. 48, no. 9, pp. 516–517, 2012.

[19] P. Unger, A. Hein, F. Demaria, M. Susanne, M. Rampp, and A. Ziegler, "Design of high-efficiency semiconductor disk lasers," Proc. SPIE 8606, pp. 860602-1–8, 2013.